# Deep Learning of Advanced Metal-Ion Batteries

Chong Yu Quan

*Faculty of Engineering, National University of Singapore*

## I. INTRODUCTION

One of the major challenges in the 21st century is the development of a consistent energy supply that is able to meet the world's growing demand for energy. Given another defining crisis of the 21st century, the climate crisis, the energy supply must be sustainable as well. However, with the present heavy dependency on fossil fuels, the energy economy at the present state is far from sustainable. Nevertheless, there have been significant efforts in tackling these immense problems through global investment from both the private and public sector in various strategies such as renewable energy sources, energy efficiency as well as novel transportation technology.

A major strategy building towards a clean and sustainable future involves the development of clean and efficient energy storage systems. From the range of solutions, electrochemical energy storage in the form of rechargeable batteries, in particular lithium-ion batteries (LIB), have since revolutionized the energy storage industry. Since its market introduction in 1991, LIB have evolved significantly, with continuously increasing energy density accompanied by decreasing cell costs [1]. Investments in the research and development of LIB in the recent decades has been largely driven by portable consumer electronics (e.g. smartphones, laptops), where LIB dominate the small portable battery market. Recently features of LIB include its implementation as the energy storage system for electric vehicles in the automotive industry as well as for stationary energy storage capable of storing excess electrical energy at a large scale with low cost [2]–[4].

However, with the intrinsic limitations of LIB, research on alternative promising battery technology is necessary given the growing differentiated demands for energy storage systems. In the next generation metal ion batteries, various novel battery compounds with different working ions, monovalent (e.g. $Na^+$, $K^+$) and multivalent (e.g. $Mg^{2+}$, $Ca^{2+}$), are proposed and intensively researched [5], [6]. However, given the wide array of working ions, such as Li, Na, K, Mg, Ca, and Al that could intercalate with different compounds, the possible battery electrodes are in the order of thousands. Majority of the electrodes have not been studied given experimental and computational difficulties in performing large chemical and structural analysis with sufficient accuracy [7]–[9]. Given such circumstances, a machine-learning (ML) approach in building models with limited computational resources to accurately predict battery electrodes properties is the most efficient way forward [10]. This approach is supported by the availability of databases and physical repositories to the scientific community with regards to useful material data (e.g. crystal structures, element-level properties) that are vital for ML. Examples of several databases include Open Quantum Materials Database (OQMD) [11], [12], Materials Project [13], [14] and Automatic Flow (AFLOW) [15] that are found in the density functional theory (DFT), which is a reasonably established computational quantum mechanical modelling method that investigates the electronic structure and properties of chemical compounds.

To date, the ML approach have been applied in various aspects of material science. For example, Deml et al. used the DFT+U-based fitted elemental-phase reference energies (FERE) approach to predict the formation enthalpy of metal-nonmetal compounds in their ground-state crystal structures [16]. Similarly, Dey et al. utilised an ensemble data mining approach involving Ordinary Least Squares (OLS), Sparse Partial Least Squares (SPLS) and Elastic Net/Least Absolute Shrinkage and Selection Operator (Lasso) regression methods coupled to Rough Set (RS) and Principal Component Analysis (PCA) methods to develop robust quantitative structure – activity relationship (QSAR) type models for band gap prediction [17]. Other applications of ML models includes crystal structure prediction [18], prediction of metal alloy properties [19], [20] and many others. In this work, the ML approach is utilised similarly for the prediction of the voltage of novel battery electrodes. The resulting predictive tool would ideally rely on the minimal basic information that are readily accessible, allowing for a rapid and accurate shortlisting of potential battery electrodes for further research and experimentation.

## II. METHODOLOGY

### *A. Training data*

One of the most important aspects of the implementation of ML material science is the selection of the appropriate input features used to represent the chemical compound. From the work of Ward et al. that builds on existing strategies found in literature, the input features of the chemical compound generally fall into 4 distinct categories: 1) stoichiometric attributes, 2) elemental property statistics, 3) electronic structure attributes, 4) ionic compound attribute [21]–[23]. Stoichiometric attributes are dependent on the fractions of the element present in the compound irregardless of the element itself. Elemental property statistics are the statistical attributes (e.g. mean, variance) of the properties of the elemental properties (e.g. atomic number, atomic radii). Electronic structure properties are the average fraction of electrons from the s, p, d and f valence shells between all present elements and ionic compound attributes are properties regarding the ionic character of the compound.

In this paper, the features used to describe a battery electrode material include the stoichiometric attributes, which are taken to be the $L^p$ norms representing the atomic fraction of the element in the battery electrode as shown in Equation 1 below.

$$\|x_p\| = (\sum_{i=0}^{n} |x_i|^p)^{\frac{1}{p}} \tag{1}$$

Adopting from the work of Ward et al., the p = 0 norm (which is equivalent to the number of components) and the p = 2, 3, 5, 7, and 10 norms [21]. The stated broad range was selected to create attributes that respond to changes in fractions with varied strengths.

Other battery electrode specific features include the working ion of the battery electrode, minimum and maximum fraction of the working ion in the battery electrode, type of metal-ion battery (e.g. intercalation) and spacegroup number. The remaining input features are the elemental properties obtained from the elemental constituents of the battery electrode adopted from the work of Joshi et al. that is also founded upon the work of Ward et al. [24]. The stated input features are readily accessible for any chemical compound with a known crystalline structure, making the model extremely easy to use.

TABLE I: Elemental Input Features

| | | | |
|---|---|---|---|
| Atomic volume | Is Mendeleev | GS band gap | Is f-block |
| Atomic number | ICSD volume | GS effective lattice constant | No. of valence |
| Atomic weight | Polarisability | GS estimated BCC lattice constant | No. of unfilled |
| Covalent radius | BCC energy difference | GS estimated FCC lattice constant | No. of s valence |
| Oxidation states | BCC effective lattice constant | GS magnetic moment | No. of d unfilled |
| Boiling temperature | BCC fermi | GS volume per atom | No. of d valence |
| Column number | BCC magnetic moment | Is metal | No. of f unfilled |
| Row number | BCC volume per atom difference | Is non-metal | No. of f valence |
| First ionization energy | BCC volume per atom | Is metalloid | No. of p unfilled |
| Space group number | Heat capacity mass | Is alkali | No. of p valence |
| Density | Heat capacity molar | Is d-block | No. of s unfilled |

Table I above states the elemental properties utilised as input features, where body centered cubic is abbreviated as BCC, ground state as GS, number as No., and Inorganic Crystal Structure Database as ICSD. For each of these elemental properties, the fraction weighted mean and average deviation are utilized to generate input features using Equation 2 and 3 respectively as shown below, where $p_i$ is the property of element i, $x_i$ is the atomic fraction, $\bar{p}$ is the mean, and $\hat{p}$ is the average deviation.

$$\bar{p} = \sum x_i p_i \tag{2}$$

$$\hat{p} = \sum x_i |p_i - \bar{p}| \tag{3}$$

The training data is obtained primarily from the Materials Project, where its database can be readily accessed through a programming interface called pymatgen [13], [14]. Another open source database, Xenonpy, is also utilised to supplement features that are otherwise unavailable in pymatgen as Xenonpy provides information from other databases such as mendeleev, CRC Hand Book and Magpie. From these databases, a total of 4401 data instances were obtained. Table II below shows the breakdown of the training data with accordance to the type of working ion in the battery electrode.

TABLE II: Training Data

| **Working Ion** | **Number of Data** | **Percentage of Total Data (%)** |
|---|---|---|
| Al | 149 | 3.39 |
| Ca | 484 | 11.00 |
| Cs | 39 | 0.89 |
| K | 125 | 2.84 |
| Li | 2291 | 52.06 |
| Mg | 393 | 8.92 |
| Na | 328 | 7.45 |
| Rb | 50 | 1.13 |
| Y | 157 | 3.58 |
| Zn | 385 | 8.75 |

From Table II, it can be observed that LIB are the majority of the battery electrodes data with 52%. Working ions of Ca, Mg, Na and Zn takes a sizeable percentage, ranging from 7% to 11% while the working ions of Al, Cs, K, Rb and Y take a small percentage, ranging from 1% to 4%. The training data then underwent pre-processing, where the categorical input features (e.g. working ion) were converted to numerical features using one-hot encoding. Given the diverse range of order of magnitude in the input features, feature scaling in necessary to ensure that gradient descent converges to the minima in an

efficient and smooth manner as well as to reduce model's biasness for input features based on magnitude. Hence, all numerical input features were standardized, giving rise to a total of 114 input features for the training data.

### *B. Hyperparmeter Optimisation*

The K-Fold cross validation methodology is utilised for hyperparameter optimisation. The training data is randomly separated into 10 folds, where 9 folds are used as the training data while the remaining fold is the holdout test set. From the training data, 10% of the data is used as the validation set for model training. The metric utilised to assess the performance of the model is the mean absolute error (MAE) as defined below in equation 4, where $Y^i_{target}$ and $Y^i_{predicted}$ are the target and predicted values for each material $i$ for training data of size $N$.

$$\bar{E} = \frac{1}{N}\sum_{n=i}^{N}\left|Y^i_{target} - Y^i_{predicted}\right| \tag{4}$$

In hyperparameter optimisation, the hyperparameters that are being optimised are the learning rate of the deep neural network, number of hidden layers and hidden units, weight-decay constant in L2 regularisation, dropout rate as well as batch size. There are various standard optimisation methods available to optimise the performance metric, which is the mean cross-validation test set MAE across 10 folds. Grid search exhaustively generates candidates from a grid of parameter values, where all the possible combinations of parameter values are evaluated and the best combination is retained. On the other hand, randomised search takes a random sample from a distribution of possible parameter values, which is more beneficial than grid search given that computational budget can be specified Furthermore, randomised search also ensures that increases in number of parameters that do not influence the performance does not decrease efficiency.

However, given that evaluating the mean cross-validation test set MAE is computationally expensive, the standard optimisations methods would take an extremely long time. Hence, a better optimisation method would be Bayesian optimisation using Gaussian processes, where the function values are assumed to follow a multivariate Gaussian. The covariance of the function values are given by a Gaussian process kernel between the parameters. Hence an efficient choice for the next parameter to be evaluate can be made by the acquisition function over the Gaussian prior, which is significantly quicker to evaluate.

TABLE III: Hyperparameters

| Hyperparameters | Lower Bound | Upper Bound | Distribution | Initial Values | Converged Values |
|---|---|---|---|---|---|
| No. of Hidden Layers | 2 | 10 | Uniform | 128 | 4 |
| No. of Hidden Units | 16 | 512 | Uniform | 5 | 398 |
| Weight Decay | $10^{-99}$ | $10^{-3}$ | Log-Uniform | $10^{-98}$ | $2.43 \times 10^{-85}$ |
| Dropout Rate | $10^{-99}$ | 0.5 | Uniform | $10^{-98}$ | 0.0142 |
| Learning Rate | $10^{-6}$ | $10^{-1}$ | Log-Uniform | $10^{-3}$ | 0.00160 |
| Batch Size | 16 | 512 | Uniform | 128 | 305 |

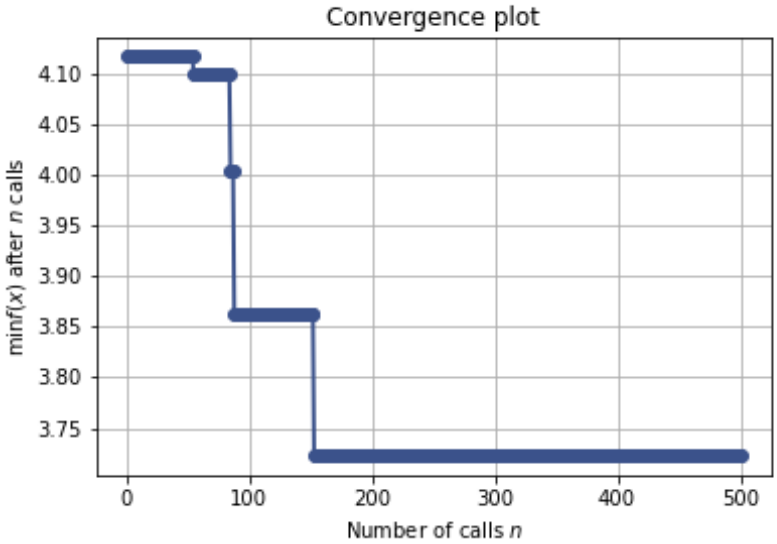


Fig. 1: Convergence plot of the objective function that outputs the sum of cross-validation test set MAE

Table III highlights the hyperparameters that are optimised, their range of values that are sampled based on their respective distribution, their initial value as well as the converged values after the optimisation process. The bounds and initial values are chosen arbitrarily based on common practices (e.g. learning rate, weight decay) as well as computational time for no. of hidden layers and units. Specifically, the lower bounds of the weight decay and dropout rate were chosen to be approximately zero ($10^{-99}$) and initialised to be $10^{-98}$. This is due to the fact that the neural network is expected to be extremely shallow. Hence, the regularisation effects of L2 regularisation and dropout would be counter-productive in the training of an effective model. This is supported by the negligibly small converged values for weight decay and dropout rate of $2.43 \times 10^{-85}$ and $0.0142$ respectively. The distribution for learning rate and rate decay are chosen to be of a logarithmic scale to ensure that the a wider range of values across different order of magnitudes are better represented.

From Figure 1, it can be observed that convergence was achieved with approximately 150 calls, which is significantly faster than most standard optimisation procedures. From the converged value as shown in Table III, the final values used in for the hyperparameters for optimised model training are as follows: No. of Hidden Layers = 4, No. of Hidden Units = 400, Weight Decay = 0, Dropout Rate = 0, Learning Rate = 0.0016 and Batch Size = 300.

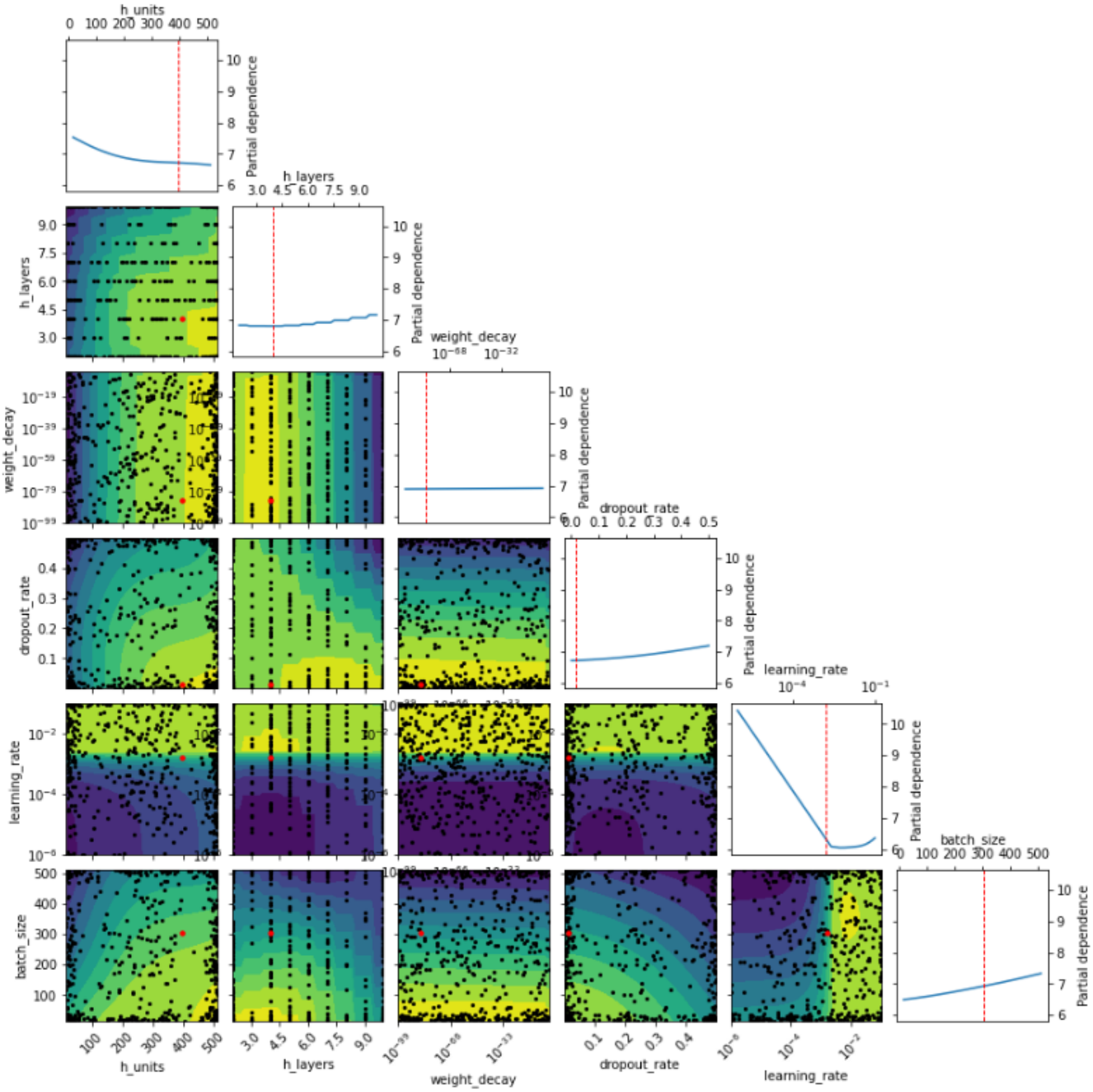


Fig. 2: Pairwise dependence plot of the objective function that outputs the sum of cross-validation test set MAE

Figure 2 shows the pairwise dependence plot of the objective function. The diagonal shows the partial dependence for the hyperparameters with respect to the objective function. The off-diagonal shows the partial dependence for two different hyperparameters with respect to the objective function. Pairwise scatter plots of the points at which the objective function was directly evaluated are shown on the off-diagonal and the red point indicates the best observed minimum.

## III. RESULTS & DISCUSSION

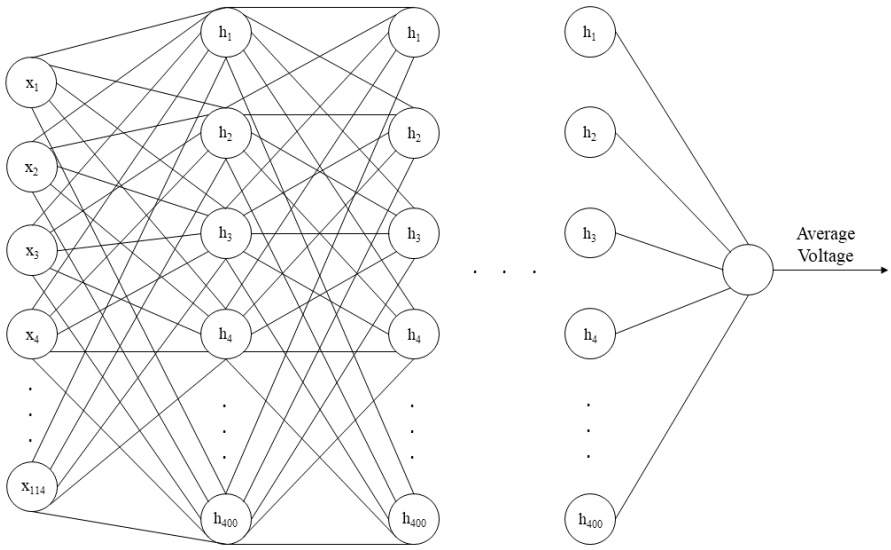


Fig. 3: Architecture of deep neural network. $x_n$ are the input features and $h_n$ is the hidden units.

Figure 3 illustrates the architecture of the deep neural network (DNN). The DNN follows a uniform architecture where the number of hidden units in the each hidden layers are the same till the one node at the output layer which predicts the average voltage. The training of the DNN follows the exact same procedures utilised in the hyperparameter tuning.

TABLE IV: Model's performance

| **Fold** | **DNN (Joshi)** | **SVR** | **KRR** | **DNN** |
|---|---|---|---|---|
| 1 | 0.42 | 0.51 | 0.54 | 0.35 |
| 2 | 0.48 | 0.25 | 0.28 | 0.34 |
| 3 | 0.42 | 0.26 | 0.27 | 0.37 |
| 4 | 0.44 | 0.35 | 0.47 | 0.34 |
| 5 | 0.44 | 0.38 | 0.43 | 0.36 |
| 6 | 0.42 | 0.62 | 0.71 | 0.37 |
| 7 | 0.43 | 0.43 | 0.42 | 0.33 |
| 8 | 0.41 | 0.59 | 0.62 | 0.41 |
| 9 | 0.45 | 0.53 | 0.57 | 0.35 |
| 10 | 0.48 | 0.28 | 0.30 | 0.38 |
| mean MAE $\pm$ standard deviation | 0.43 $\pm$ 0.03 | 0.42 $\pm$ 0.13 | 0.46 $\pm$ 0.14 | 0.36 $\pm$ 0.02 |

Table IV shows the results of the trained DNN against results from the work of Joshi et al., where they compared their DNN model's performance with other ML models such as support vector regression (SVR) and kernel ridge regression (KRR) [24]. SVR is a kernel-based regression technique that operates by mapping nonlinearly separable data in real space to higher dimensional space through a hyperplane constructed by a kernel function. Similar to SVR, KRR combines ridge regression (linear least squares with l2-norm regularization) with the kernel trick to map nonlinearly separable data in real space to higher dimensional space through a hyperplane constructed by a kernel function. In the work of Joshi et al., the models trained using SVR and KRR underwent hyperparameter optimisation using grid search and are robust alternatives to DNN for complex datasets. Nevertheless, it can be observed that the trained DNN has the lowest mean MAE relative to other models utilised. The trained DNN mean MAE of 0.36 is a 16% reduction from the mean MAE of 0.43 of the DNN in the work of Joshi et al., which is a significant reduction. It can also be seen that the DNN models are generally more consistent given significantly smaller standard deviation as compared to those of SVR and KRR.

TABLE V: Model's performance across working ions

| Working Ion | Number of Data | Percentage of Total Data (%) | Mean MAE |
|---|---|---|---|
| Al | 149 | 3.39 | 0.11 |
| Ca | 484 | 11.00 | 0.10 |
| Cs | 39 | 0.89 | 0.16 |
| K | 125 | 2.84 | 0.12 |
| Li | 2291 | 52.06 | 0.12 |
| Mg | 393 | 8.92 | 0.38 |
| Na | 328 | 7.45 | 0.10 |
| Rb | 50 | 1.13 | 0.15 |
| Y | 157 | 3.58 | 0.09 |
| Zn | 385 | 8.75 | 0.13 |

Table V highlights the model's performance for each working ion data set. It can be observed that mean MAE for the all working ions falls within the range of 0.09 - 0.16, with the exception of $Mg^{2+}$ of 0.38. This is an unexpected outcome given that mean MAE for Rb, which accounts for 1.13% of the data set is approximately similar to that of Li, which accounts for 52.06% of the data set. A plausible explanation for such a discrepancy could potentially be due to significantly commonality between working ion's data other than $Mg^{2+}$. As a result, the model learned weights geared to minimize the MAE favouring the majority of the working ions, which happened to perform relatively poorly for $Mg^{2+}$.

Despite the consistent performance of the trained DNN, the true challenge for it would be to gauge its performance from a completely new data set with labels based on experimentally determined voltage values instead of the average voltage obtained from Materials Project. This is necessary to ensure the transferability and robustness of the trained DNN. Table VI shows the trained model predictions against the DNN model on selected experimental data from the work of Joshi et al. [24].

TABLE VI: Model's performance on experimental data

| Electrode | DNN (Joshi) | DNN | Experimental | Absolute Error (Joshi) | Absolute Error |
|---|---|---|---|---|---|
| $NaMnO_2$ | 2.98 | 2.92 | 2.75[a] | 0.23 | 0.17 |
| $NaCoO_2$ | 3.40 | 3.10 | 2.80[b] | 0.60 | 0.30 |
| $NaTiO_2$ | 1.79 | 1.21 | >1.50[b] | 0.29 | 0.29 |
| $NaNiO_2$ | 3.61 | 3.05 | 3.00[b] | 0.61 | 0.05 |
| $NaFePO_4$ | 2.95 | 4.06 | 3.00[b] | 0.05 | 1.06 |
| $NaFe_{0.5}Co_{0.5}O_2$ | 3.58 | 3.16 | 3.14[d] | 0.44 | 0.02 |
| $Na_4MnV(PO_4)_3$ | 3.42 | 3.14 | 3.00[c] | 0.42 | 0.14 |
| | | | **MAE (Na)** | **0.38** | **0.29** |
| $LiCoO_2$ | 3.60 | 3.98 | 4.10[b] | 0.50 | 0.12 |
| $LiFePO_4$ | 3.36 | 4.26 | 3.50[b] | 0.14 | 0.76 |
| $LiNiO_2$ | 3.81 | 3.88 | 3.85[b] | 0.04 | 0.03 |
| | | | **MAE (Li)** | **0.23** | **0.30** |
| $Mg_2Mo_6S_8$ | 1.09 | 1.48 | 1.30[f] | 0.21 | 0.18 |
| $Mg_{0.55}TiSe_2$ | 1.63 | 0.83 | 1.45[g] | 0.18 | 0.62 |
| $MgMoO_3$ | 2.20 | 3.43 | 2.25[h] | 0.05 | 1.18 |
| | | | **MAE (Mg)** | **0.15** | **0.66** |
| $K_{1.6}Na_2Mn_3O_7$ | 2.74 | 3.15 | 2.20[e] | 0.54 | 0.95 |
| | | | **MAE (All)** | **0.31** | **0.42** |

* [a]Taken from ref [25]. [b]Taken from ref [26]. [c]Taken from ref [27]. [d]Taken from ref [28]. [e]Taken from ref [29]. [f]Taken from ref [30]. [g]Taken from ref [31] [h]Taken from ref [32].

From Table VI, it can be observed that the trained model's performance on the experimental data has deteriorated slightly relative to its test set performance as shown in Table IV. On the other hand, the DNN model from the work of Joshi et al. performed slightly better on the experimental data relative to its test set performance. Upon further inspection, it would appear than the trained model's poorer performance on $Mg^{2+}$ is also evident given its performance from the $Mg^{2+}$ experimental data. Furthermore, it can be seen that the standard deviation of MAE of the trained model is larger than that from the DNN from Joshi et al.. In particular, it can be observed that the absolute error for some anomalous electrodes (e.g. $NaFePO_4$, $MgMoO_3$, $LiFePO_4$, $Mg_{0.55}TiSe_2$, $K_{1.6}Na_2Mn_3O_7$) have absolute errors close to 1 or above while the absolute errors for Joshi et al. are significantly smaller. Hence, this could be an indication of potential overfitting in the trained model where the potential corrections include regularisation techniques such as L2 regularisation and weight decay discussed previously. However, given such a small sample of experimental data with 14 data points where the working ions are mainly Na, Li and Mg, the respective

models' performance cannot be fully ascertained. A potential hypothesis for the anomalous results stated before would be that the anomalies are a result of an inherent trade off that the model made in order to improve its performance in general for a wider scope of electrodes of varying working ions and anions at the expense of significantly poorer performance for a smaller and more specific subsets of electrodes (e.g. electrodes with anions of $FePO_4^-$ or $Mg^{2+}$ working ions). This is corroborated by the at minimum equivalent or significantly better performance of the trained model for the other experimental electrodes relative to the to the model from from Joshi et al (e.g. $NaNiO_2$, $NaFe_{0.5}Co_{0.5}O_2$, $LiCoO_2$) as well as the result shown in Table IV. As a result, future studies on a larger and more diverse data set on novel experimental electrodes is necessary to fully evaluate the model's performance and ascertain the stated hypothesis above in order to decide the best methods in improving the model.

## IV. CONCLUSION

In conclusion, this project utilises DNN to train a model capable of predicting the voltage of battery electrodes using materials data that are primarily extracted from the Material's Project. A prediction can be obtained using readily available basic information: working ion of the battery electrode, minimum and maximum fraction of the working ion in the battery electrode, type of metal-ion battery (e.g. intercalation) and spacegroup number. The remaining input are the elemental properties obtained from the elemental constituents of the battery electrode, making the model simple and efficient compared to DFT methods. Hence, the trained model from this project can be used to rapidly shortlist potential high performing battery electrodes for further experimentation, streamlining the research and development process in this field. However, further improvements must be made to the existing model to improve the model's performance for application in reality. Potential improvements would include training with a larger data sets, exploring different ML algorithms and input features. As such, many unexplored possibilities and potential lies in the ML approach as room for further research and development.

## REFERENCES


[1] A. Thielmann, A. Sauer, and M. Wietschel, "Fraunhofer-institute isi," 2015.

[2] G. E. Blomgren, "The development and future of lithium ion batteries," *Journal of The Electrochemical Society*, vol. 164, no. 1, p. A5019, 2016.

[3] D. Andre, S.-J. Kim, P. Lamp, S. F. Lux, F. Maglia, O. Paschos, and B. Stiaszny, "Future generations of cathode materials: an automotive industry perspective," *Journal of Materials Chemistry A*, vol. 3, no. 13, pp. 6709–6732, 2015.

[4] G. Patry, A. Romagny, S. Martinet, and D. Froelich, "Cost modeling of lithium-ion battery cells for automotive applications," *Energy Science & Engineering*, vol. 3, no. 1, pp. 71–82, 2015.

[5] P. K. Nayak, L. Yang, W. Brehm, and P. Adelhelm, "From lithium-ion to sodium-ion batteries: advantages, challenges, and surprises," *Angewandte Chemie International Edition*, vol. 57, no. 1, pp. 102–120, 2018.

[6] T. Placke, R. Kloepsch, S. Dühnen, and M. Winter, "Lithium ion, lithium metal, and alternative rechargeable battery technologies: the odyssey for high energy density," *Journal of Solid State Electrochemistry*, vol. 21, no. 7, pp. 1939–1964, 2017.

[7] P. Kirkpatrick and C. Ellis, "Chemical space," *Nature*, vol. 432, no. 7019, p. 823, 2004.

[8] O. A. Von Lilienfeld, "Quantum machine learning in chemical compound space," *Angewandte Chemie International Edition*, vol. 57, no. 16, pp. 4164–4169, 2018.

[9] A. Mullard, "The drug-maker's guide to the galaxy," *Nature News*, vol. 549, no. 7673, p. 445, 2017.

[10] M. I. Jordan and T. M. Mitchell, "Machine learning: Trends, perspectives, and prospects," *Science*, vol. 349, no. 6245, pp. 255–260, 2015.

[11] J. E. Saal, S. Kirklin, M. Aykol, B. Meredig, and C. Wolverton, "Materials design and discovery with high-throughput density functional theory: the open quantum materials database (oqmd)," *Jom*, vol. 65, no. 11, pp. 1501–1509, 2013.

[12] S. Kirklin, J. E. Saal, B. Meredig, A. Thompson, J. W. Doak, M. Aykol, S. Rühl, and C. Wolverton, "The open quantum materials database (oqmd): assessing the accuracy of dft formation energies," *npj Computational Materials*, vol. 1, no. 1, pp. 1–15, 2015.

[13] A. Jain, S. P. Ong, G. Hautier, W. Chen, W. D. Richards, S. Dacek, S. Cholia, D. Gunter, D. Skinner, G. Ceder *et al.*, "Commentary: The materials project: A materials genome approach to accelerating materials innovation," *Apl Materials*, vol. 1, no. 1, p. 011002, 2013.

[14] S. P. Ong, W. D. Richards, A. Jain, G. Hautier, M. Kocher, S. Cholia, D. Gunter, V. L. Chevrier, K. A. Persson, and G. Ceder, "Python materials genomics (pymatgen): A robust, open-source python library for materials analysis," *Computational Materials Science*, vol. 68, pp. 314–319, 2013.

[15] S. Curtarolo, W. Setyawan, G. L. Hart, M. Jahnatek, R. V. Chepulskii, R. H. Taylor, S. Wang, J. Xue, K. Yang, O. Levy *et al.*, "Aflow: an automatic framework for high-throughput materials discovery," *Computational Materials Science*, vol. 58, pp. 218–226, 2012.

[16] A. M. Deml, R. O'Hayre, C. Wolverton, and V. Stevanović, "Predicting density functional theory total energies and enthalpies of formation of metal-nonmetal compounds by linear regression," *Physical Review B*, vol. 93, no. 8, p. 085142, 2016.

[17] P. Dey, J. Bible, S. Datta, S. Broderick, J. Jasinski, M. Sunkara, M. Menon, and K. Rajan, "Informatics-aided bandgap engineering for solar materials," *Computational Materials Science*, vol. 83, pp. 185–195, 2014.

[18] S. Curtarolo, D. Morgan, K. Persson, J. Rodgers, and G. Ceder, "Predicting crystal structures with data mining of quantum calculations," *Physical review letters*, vol. 91, no. 13, p. 135503, 2003.

[19] H. Bhadeshia, R. Dimitriu, S. Forsik, J. Pak, and J. Ryu, "Performance of neural networks in materials science," *Materials Science and Technology*, vol. 25, no. 4, pp. 504–510, 2009.

[20] S. Chatterjee, M. Murugananth, and H. Bhadeshia, "$\delta$ trip steel," *Materials Science and Technology*, vol. 23, no. 7, pp. 819–827, 2007.

[21] L. Ward, A. Agrawal, A. Choudhary, and C. Wolverton, "A general-purpose machine learning framework for predicting properties of inorganic materials," *npj Computational Materials*, vol. 2, no. 1, pp. 1–7, 2016.

[22] L. M. Ghiringhelli, J. Vybiral, S. V. Levchenko, C. Draxl, and M. Scheffler, "Big data of materials science: critical role of the descriptor," *Physical review letters*, vol. 114, no. 10, p. 105503, 2015.

[23] B. Meredig, A. Agrawal, S. Kirklin, J. E. Saal, J. Doak, A. Thompson, K. Zhang, A. Choudhary, and C. Wolverton, "Combinatorial screening for new materials in unconstrained composition space with machine learning," *Physical Review B*, vol. 89, no. 9, p. 094104, 2014.

[24] R. P. Joshi, J. Eickholt, L. Li, M. Fornari, V. Barone, and J. E. Peralta, "Machine learning the voltage of electrode materials in metal-ion batteries," *ACS applied materials & interfaces*, vol. 11, no. 20, pp. 18 494–18 503, 2019.

[25] J. Billaud, R. J. Clément, A. R. Armstrong, J. Canales-Vázquez, P. Rozier, C. P. Grey, and P. G. Bruce, "$\beta$-namno2: a high-performance cathode for sodium-ion batteries," *Journal of the American Chemical Society*, vol. 136, no. 49, pp. 17 243–17 248, 2014.

[26] S. P. Ong, V. L. Chevrier, G. Hautier, A. Jain, C. Moore, S. Kim, X. Ma, and G. Ceder, "Voltage, stability and diffusion barrier differences between sodium-ion and lithium-ion intercalation materials," *Energy & Environmental Science*, vol. 4, no. 9, pp. 3680–3688, 2011.

[27] U. Nisar, R. Shakoor, R. Essehli, R. Amin, B. Orayech, Z. Ahmad, P. R. Kumar, R. Kahraman, S. Al-Qaradawi, and A. Soliman, "Sodium intercalation/de-intercalation mechanism in na4mnv (po4) 3 cathode materials," *Electrochimica Acta*, vol. 292, pp. 98–106, 2018.
[28] H. Yoshida, N. Yabuuchi, and S. Komaba, "Nafe0. 5co0. 5o2 as high energy and power positive electrode for na-ion batteries," *Electrochemistry communications*, vol. 34, pp. 60–63, 2013.
[29] K. Sada, B. Senthilkumar, and P. Barpanda, "Potassium-ion intercalation mechanism in layered na2mn3o7," *ACS Applied Energy Materials*, vol. 1, no. 10, pp. 5410–5416, 2018.
[30] P. Canepa, G. Sai Gautam, D. C. Hannah, R. Malik, M. Liu, K. G. Gallagher, K. A. Persson, and G. Ceder, "Odyssey of multivalent cathode materials: open questions and future challenges," *Chemical reviews*, vol. 117, no. 5, pp. 4287–4341, 2017.
[31] Y. Gu, Y. Katsura, T. Yoshino, H. Takagi, and K. Taniguchi, "Rechargeable magnesium-ion battery based on a tise 2-cathode with d-p orbital hybridized electronic structure," *Scientific reports*, vol. 5, no. 1, pp. 1–9, 2015.
[32] G. Gershinsky, H. D. Yoo, Y. Gofer, and D. Aurbach, "Electrochemical and spectroscopic analysis of mg2+ intercalation into thin film electrodes of layered oxides: V2o5 and moo3," *Langmuir*, vol. 29, no. 34, pp. 10 964–10 972, 2013.